Polar and Hydrophobic Pores and Channels in Peptide Assemblies

I.L. Karle
Laboratory for Structure of Matter

Introduction: The formation of pores, channels, and nanotubes by the assembly of a number of individual like-molecules into larger entities results in properties that the individual molecules do not possess. These assemblies enable, for example, charged ions to pass through hydrophobic membranes, or permit the insertion of hydrophobic molecules into nonpolar pores to render them soluble in media in which they would be otherwise insoluble. The discussion and examples shown in this paper are limited to one class of natural peptides and to hybrid peptides in which macrocycles are formed from peptide segments that are interspersed with one or more organic scaffolds. Voltage-gated ion transport peptides, often functioning as antibiotics, have been found to occur in nature in the lower forms of life, such as fungi. They form ion channels in the shape of funnels or hourglasses by the assembly of three or more bent amphiphilic helices.[1] These channels have a polar interior wall containing carbonyl moieties and a hydrophobic exterior surface composed of methyl groups. An entirely different motif exists for forming channels or tubes from peptides or peptide hybrids in which the backbone is in the form of a macrocycle with 12 or more atoms in the ring. In this motif, the macrocycles stack over each other with their C=O and NH moieties in sufficient register to permit C=O···HN hydrogen bonds to be formed. Infinite, open-ended tubules are formed in the direction of the stacking in which the walls of the tubes are the hydrogen bonds.

Methods: The geometric parameters describing the structures of the molecules, as well as the folding, twisting, packing, and assembly of molecules are established by single crystal X-ray diffraction procedures.

Results and Discussion: *Ion channel formers that occur in nature*—Zervamicin and the related antiamoebin, 16-residue peptides found in spores in the soil,[1] transport K^+ ions through lipophilic membranes by channel formation. Each molecule folds into a severely bent amphiphilic helix, Fig. 1(a). The hourglass-shaped channels are filled with water molecules that form hydrogen bonds among themselves and with the polar side chains or carbonyls that extend into the channel, such as the carbonyls of Hyp^{10} and Hyp^{13}.* The channel formed by three helical molecules, Fig. 1(a), is closed at the waist-line by a trans-channel hydrogen bond between the terminal N^{ε} atom of Gln^{11}† in one helix and the O of the OH group of Hyp^{10} in another helix. This hydrogen bond occurs sequentially in a "closed" and "open" conformation for the passage of each K^+ ion, Fig. 1(b). Remarkably, both positions have been found in the same crystal of zervamicin in an 80:20 ratio. Figure 1(b) is a schematic diagram of a possible path for a K^+ ion that involves a double-gating mechanism. The chosen path has a continuous cross-section of at least 5.6 Å, a value that allows pairs of K^+—O ligands at 2.8 Å to form fleetingly during the passage.

Construction of nonpolar tubules with model peptides—The construction of hollow tubules (such as indicated in the Introduction) has not been successful with cyclic peptides containing only α-amino acid residues and having the same chirality (all L- or all D-handed).†† Tubules consisting only of cyclic peptides have been constructed successfully, and their crystal structures have been determined with the following motifs in the cyclic peptides: alternating α- and β-amino acids, all β-amino acids and alternating D- and L- amino acids.

In an attempt to construct tubules with adjustable diameters, macrocycles were synthesized in which peptide segments were alternated with organic scaffolds. Successful tubule formers were the polymethylene-bridged cystine-based cyclo bisureas (Fig. 2(a)) and cyclo bisamides (Fig. 3). Molecules in these families formed relatively planar rings with C=O and NH moieties approximately perpendicular to the plane of the rings. In the crystals in Fig. 2, the molecules stack over each other and are held together by urea-type hydrogen bonding on either side of the ring. In the bisamides in Fig. 3, the hydrogen bonding is a linear repetition along a strand. Similar tubules are formed for members of each family. The tubules are characterized by three rigid walls consisting of opposing walls containing the hydrogen bonds and one connecting wall containing the disulfide moiety. The fourth wall consists of the polymethylene linker with a variable number of CH_2 groups. It is the fourth wall that determines the size of the cavity in the tubule, depending on the length of the polymethylene chain that had been selected, from n = 4 to ~20 (Fig. 3). It should be noted that the polymethylene chain is quite flexible and usually has

*Hyp ≡ hydroxyproline
†Gln ≡ glutamine
††D ≡ dextro (right-handed); L ≡ levo (left-handed)

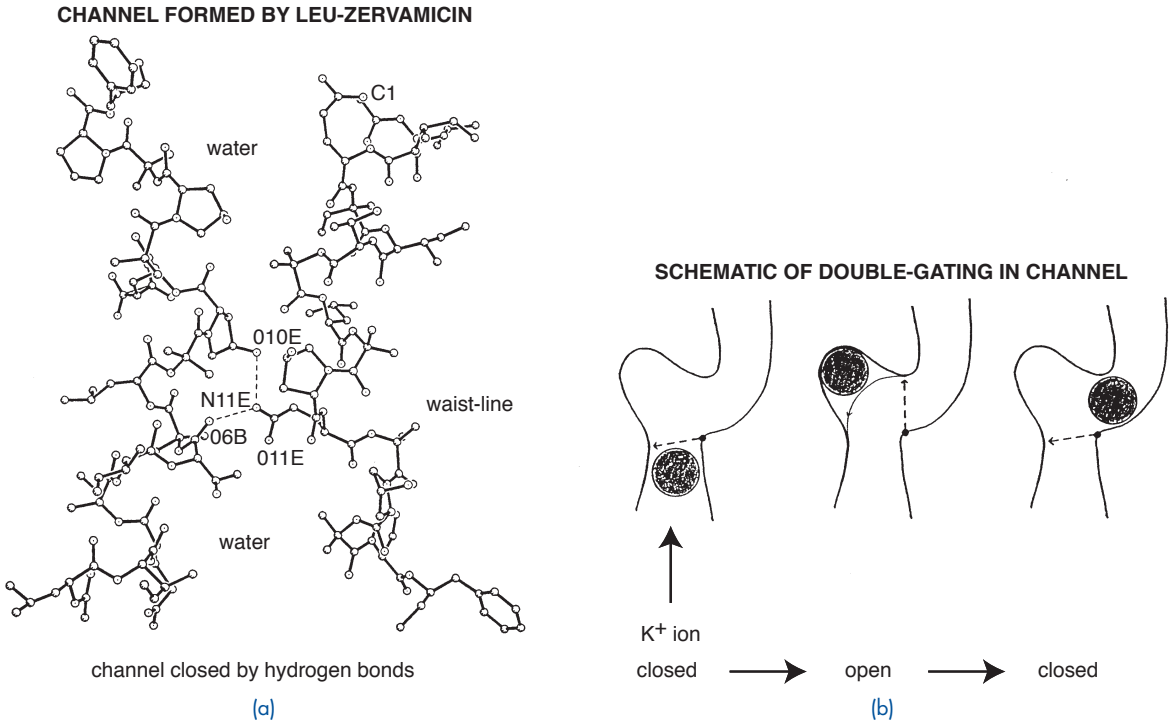

FIGURE 1
(a) Hourglass shaped channel, with a polar interior, of antibiotic molecules (only two are shown) that transports potassium ions through cell membranes. (b) Upon application of a small potential, the gate at residue 11 is opened by the rotation of the side chain at 11 to another position that allows partial passage of the K^+ ion. The gate must close again before the K^+ ion can continue its passage.

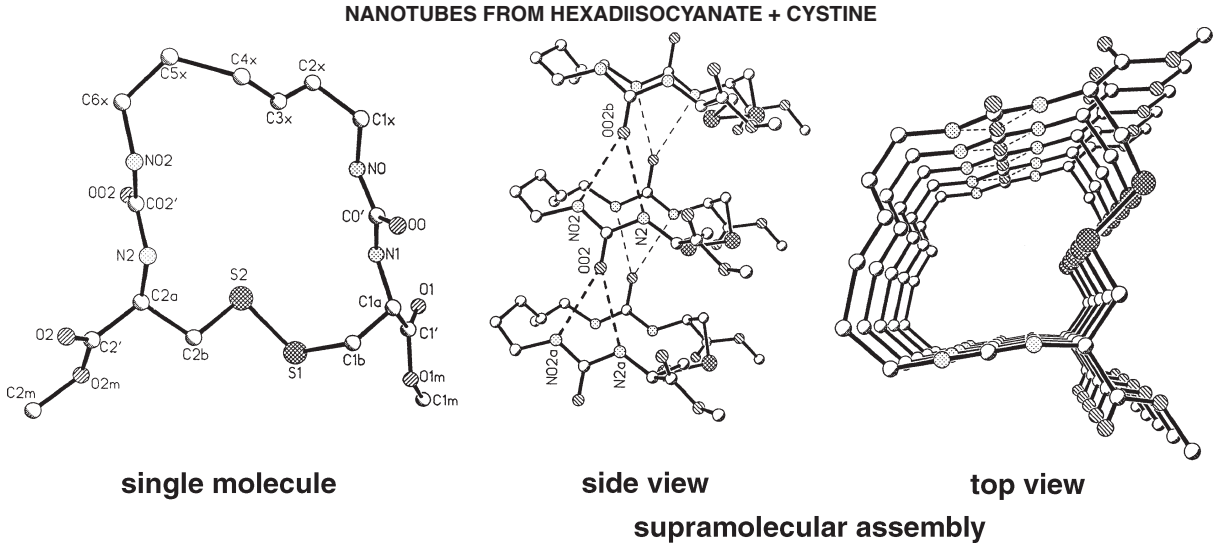

FIGURE 2
Macrocycles that stack and self-assemble into infinite tubules by urea-type hydrogen bonding (crystal structure analysis). The upper wall of the molecule, composed of flexible methylene chains, may vary in length from 4 to ~20 CH_2 groups.

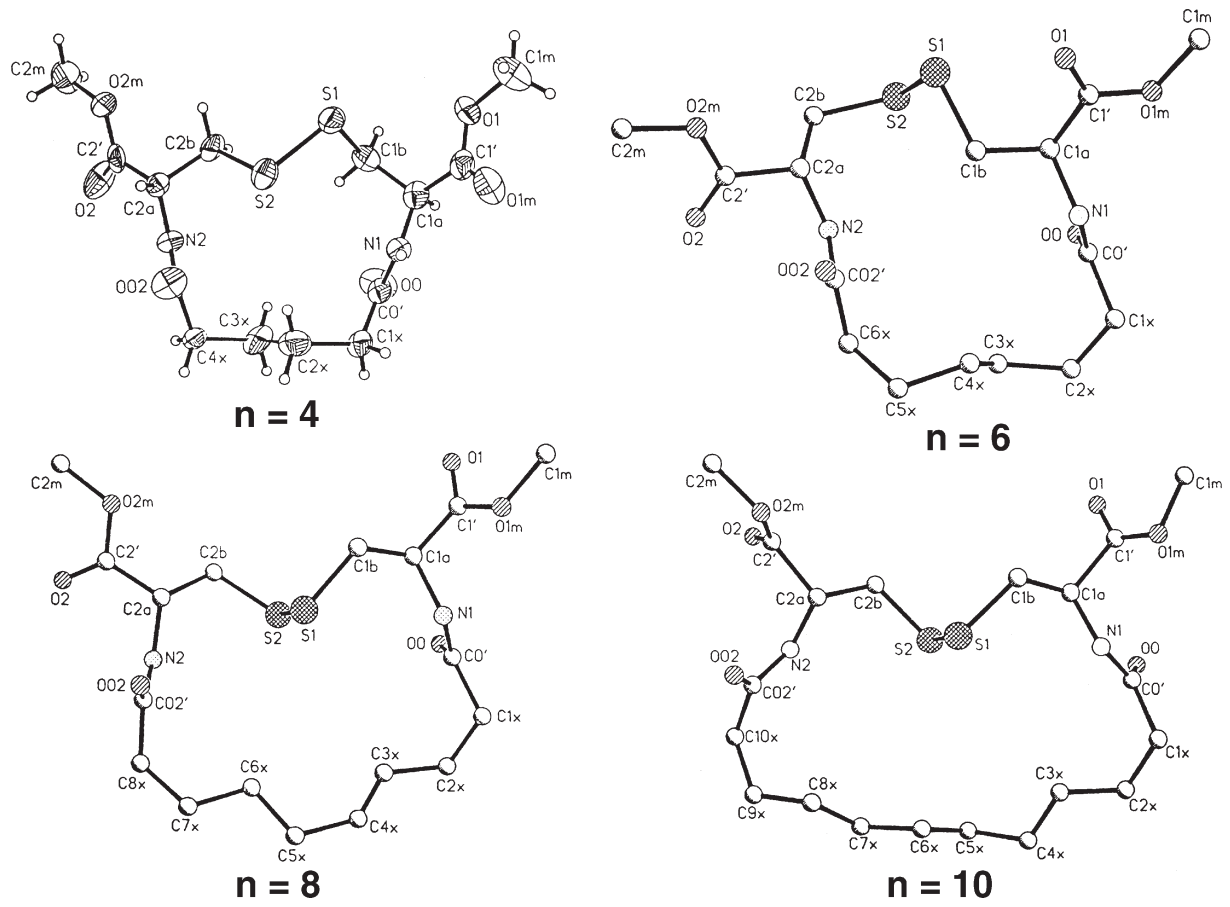

FIGURE 3
Family of macrocycles that stack and self-assemble into infinite tubules by amide-type hydrogen bonding. The tubules differ from the urea-type shown in Fig. 2 by the removal of an NH group from each vertical side of cyclic backbones. Cavity in the tubules enlarges with the lengthening of the methylene chain.

some disorder. The cavity does not collapse with longer polymethylene chains, but rather maintains a shape with empty space. This is an unusual occurrence considering that moderate and large macrocycles formed by cyclization of peptides have rarely been observed to form large open pores. More frequently, the interior space collapses to some minimum space, accompanied by folding of the backbone and formation of intracyclic NH···OC hydrogen bonds.

No electron density is found inside the tubules, which attests to their empty state. Furthermore, unlike the channels in the peptide ionophores (above) these oval cavities have a hydrophobic lining. The interior behaves like an apolar organic solvent and can enhance the solubility in water of highly lipophilic substances by selective guest-host interactions. For example, the tubule with $n = 20$ can solubilize pyrene, perylene, and the dye Nile Red, whereas tubules of the same family, but with shorter polymethylene linkers and therefore smaller cavities cannot.[2]

Conclusions: This article describes synthetic hybrid peptide macrocycles with empty interior space and the propensity to stack, resulting in the formation of endless open tubules with NH···OC hydrogen bonds as important support struts in the tubule walls. The cystine residue appears to provide a sufficiently rigid scaffold for the remainder of the macrocycle to prevent the collapse of the empty space within the macrocycle. Flexibility in the long polymethylene chains in compounds forming the successful tubules, manifested by disorder in the crystal structures, may facilitate the entry process of hydrophobic guest molecules into the interior of the tubules.

Acknowledgements: I wish to acknowledge the collaboration of Dr. Darshan Ranganathan of Discovery Laboratory, Indian Institute of Chemical Technology, Hyderabad, India, for design and synthesis of the hybrid peptides, and Prof. P. Balaram of the Molecular Biophysics Unit, Indian Institute of Science,

Bangalore, India, for the isolation and crystallization of the antibiotic peptides.

[Sponsored by ONR and NIH]

References

[1] I.L. Karle, M.A. Perozzo, V.K. Mishra, and P. Balaram, "Crystal Structure of the Channel-Forming Polypeptide Antiamoebin in a Membrane-Mimetic Environment," *Proc. Natl. Acad. Sci. USA* **95**, 5501-5504 (1998).

[2] D. Ranganathan, V. Haridas, C.S. Sundari, D. Balasubramanian, K.P. Madhusudanan, R. Roy, and I.L. Karle, "Design, Synthesis, Crystal Structure, and Host-Guest Properties of Polymethylene-Bridged Cystine-Based Cyclobisamides: A Facile Entry into Hydrogen-Bonded Peptide Nanotubes," *J. Org. Chem.* **64,** 9230-9240 (1999).

Remote Tank Monitoring and Inspection Methods

E. Lemieux, A. Webb, K.E. Lucas, P.F. Slebodnick, M. Krupa, and F. Martin
Chemistry Division

E.A. Hogan
Materials Science and Technology Division

Summary: Preservation of tanks and voids on U.S. Navy ships expends more than 25% of maintenance funds annually. The MIL-P-24441 system that has been installed in most tanks and voids has a 5 to 7-year service life. Two major thrusts have been made to reduce maintenance costs of tank and void preservation: (1) replacement with high solid epoxy coating systems that are approximately 98% solids, are edge-retentive, and have a service life of 20 years; and (2) implementation of condition-based maintenance technology via electrochemical in situ sensors and remote optical inspection technologies for routine assessment of the "state of preservation" of shipboard tanks and voids. This article reviews improvements in technology currently being developed with regard to the second thrust area. Various inspection techniques, including the Insertable Stalk Imaging System (ISIS), the Remotely Operated Paint Inspector (ROPI), and the Corrosion Detection Algorithm (CDA) are discussed.

Introduction: Ballast tank spaces include seawater tanks for ballast and damage control, compensated fuel tanks, fuel/oil service, potable water storage, and combined holding tanks (CHT). These spaces have coatings as the primary corrosion control element and a cathodic protection system as the secondary element to minimize coating degradation and effects of galvanic corrosion. Currently, U.S. Navy maintenance practices for ballast tank spaces include Fleet-wide inspection of the 20,000 tanks. Approximately 4,000 of these occur annually, at a conservative cost of $24M. Inspection typically requires the opening of all tank hatches, cleaning, maintenance of a gas-free environment, and entry of trained personnel to evaluate tank integrity. Operationally, each tank may see different degrees of service depending on mission requirements, thus creating widely variable maintenance concerns, in addition to those problems routinely anticipated for each tank type. As a result, up to 50% of current tank maintenance is due to hidden damage or unplanned work. Costs for tanks identified for refurbishment soar to $250M/year for a fraction of the total tanks Fleet-wide.

NRL has developed a strategy by which the "state of preservation" can be determined by the implementation of Tank Monitoring Systems (TMS), which is essentially an unmanned tank entry method for inspection and qualification of tank integrity. The TMS systems include (1) an in-situ corrosion sensor (Fig. 4), which is installed in the tank to monitor coating integrity, the corrosion status, and cathodic protection functionality; (2) insertable optical systems (Fig. 5), for periodic remote visual and analytical assessment of coatings damage; and (3) software to integrate the results of the corrosion sensor and optical measurements, which allow maintenance needs and dollars to be predicted and assessed on a "condition basis" rather than the traditional "time interval" method.

Optical Inspection Techniques: The optical systems of the TMS strategy include three significant elements, an Insertable Stalk Inspection System (ISIS); a Remotely Operated Vehicle (ROV) for remote inspection termed the Remotely Operated Paint Inspector (ROPI); and an image analysis software package utilized as the Corrosion Detection Algorithm (CDA). ISIS currently incorporates a 72:1 zoom-capable charge-coupled device (CCD) camera, 70-W lighting, a hatch-mountable pole (stalk) for camera insertion, and a video recording device. ISIS is inserted up to 3 m into the tank through a personnel entry hatch and is mounted to the hatch. The operator then records high-resolution images (stills) and video of all tank surfaces for later analysis.

The ROPI system, is essentially a mini-ROV, whose dimensions allow entry through the ~ 13 × 21-in. tank hatches. The ROPI is ideal for use in tanks that are ballasted and those having numerous obstructions that would prevent useful implementation of the ISIS system. The ROPI is outfitted with an autohover system that will allow for smooth vertical evaluation of tank surfaces. A total 340 W of lighting with intensity control are included onboard for adequate lighting in a variety of conditions. As in the ISIS sys-

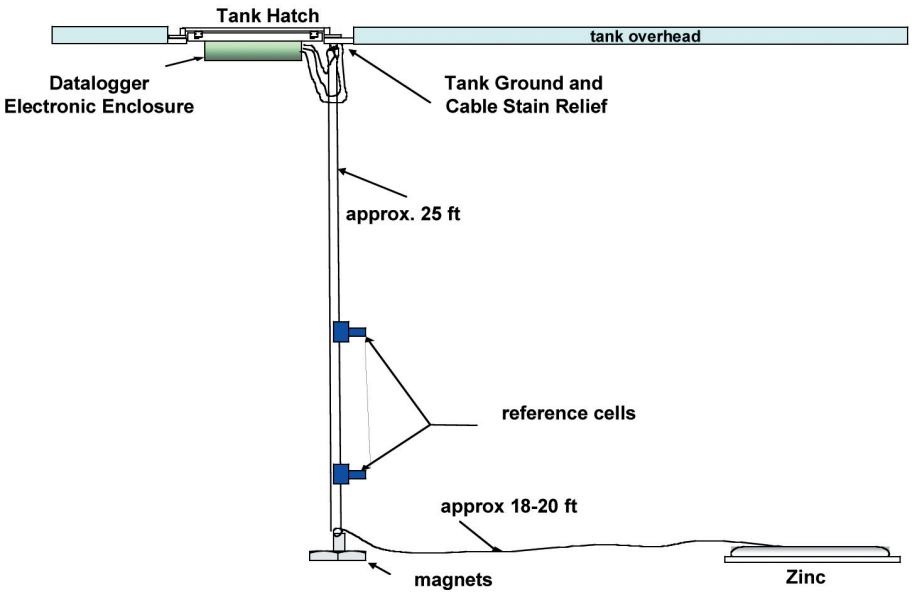

FIGURE 4
Schematic of the corrosion sensor for remote monitoring of tanks and voids.

Remotely Operated Paint Inspector

Insertable Stalk Imaging System

FIGURE 5
Remote Tank Inspection Hardware.

tem, a zoom-operable CCD camera is also onboard. One of the unique features afforded the ROPI is the inclusion of dual reference electrodes that measure the tank condition from a corrosion standpoint. These corrosion sensors provide a number of advantages over both the TMS sensor and ISIS in that both a global view of the tank condition and highly localized measurements can be obtained in mission-critical spaces. In addition, these sensors ascertain whether the cathodic protection system is adequately controlling corrosion. The data obtained from the reference electrode are integrated with the video so that the condition is immediately viewable with the image.

Finally, the CDA provides an analytical tank assessment from acquired video imagery to provide the coatings inspector with a "percent damaged" coating, an example of which is shown in Fig. 6. With the use of ROPI and ISIS in conjunction with the CDA, it is expected that a repeatable and objective evaluation of the coatings damage can be achieved. This represents a significant development in tank coatings inspection since, to date, human inspectors have been expected to accurately distinguish tank damage from 0 to 10% within 1% of the actual. This ability is not only difficult but is subjective, especially where different inspectors are used.

Conclusions: Ship husbandry using TMS, either as individual elements or as an integrated system will provide the U.S. Naval Fleet a useful tool by which a variety of tanks and their coatings systems can be evaluated on a regular basis without manned

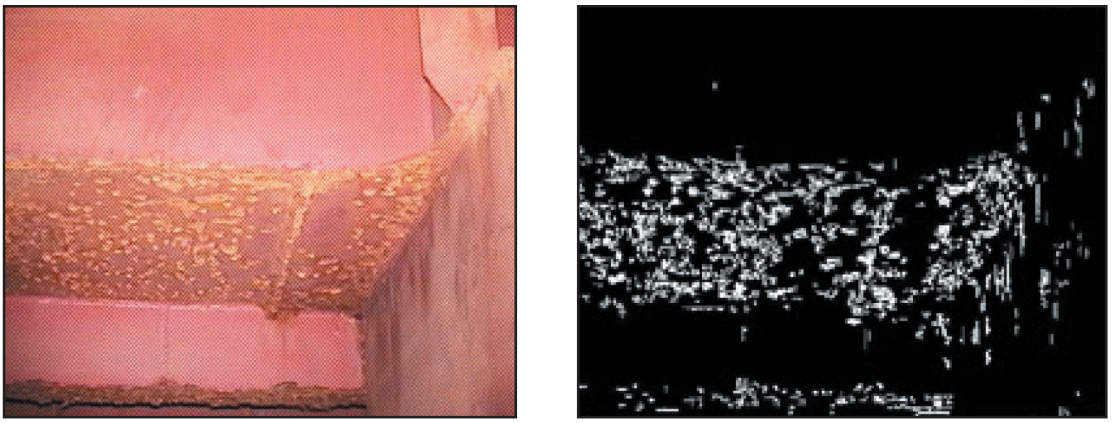

FIGURE 6
Original image (left) and analyzed image (right) revealing a 7.1% damage.

entry. In addition, these components will significantly reduce the manpower and costs associated with tank inspection and preservation and minimize the high costs of unplanned tank represervation.

Acknowledgments: The authors gratefully acknowledge the support, coordination, and guidance provided by NAVSEA 05N and 05M in performing much of the work discussed in this paper. Specifically, the authors acknowledge the many contributions provided by Captain William Needham, Mr. E. Dail Thomas, and Mr. Andy Seelinger.

[Sponsored by NAVSEA]

Ocean Floor Methane Gas Hydrate Exploration

R.B. Coffin,[1] R. Lamontagne,[1] S. Rose-Pehrsson,[1] K.S. Grabowski,[2] D.L. Knies,[2] S.B. Qadri,[2] J. P. Yesinowski,[1] J.W. Pohlman,[3] M. Yousuf,[4] and J.A. Linton[5]

[1]*Chemistry Division*
[2]*Materials Science and Technology Division*
[3]*Geocenters, Inc.*
[4]*George Washington University*
[5]*Argonne National Laboratory*

Introduction: Over the last decade, large deposits of methane hydrates have been identified along the world continental margins. Frozen mixtures of hydrocarbon gas (mostly methane) and water occur over large areas of the ocean floor and vastly exceed other carbon-energy reservoirs. With a maximum content of 164 m^3 of methane and 0.8 m^3 of water at standard temperature and pressure per cubic meter of hydrate and an estimated range of 26 to 139 $\times$ 10^{15} m^3 globally, this is a significant new energy source. The content of methane in hydrates is variable and is controlled by geothermal gradients and biological methane production. International research has begun, with a primary goal of obtaining the methane in these hydrates as an energy source.

This requires a broad range of scientific efforts to address the methane hydrate presence, develop mining strategies, and predict the impact on the environment and platform stability. The Naval Research Laboratory (NRL) has developed strong research topics regarding methane hydrates over the last 30 years. NRL has unique field and laboratory expertise that couples physical, chemical, and biological parameters to address methane hydrate distribution, formation, and stability. Recent, current, and planned field work is active on the Texas-Louisiana Shelf in the Gulf of Mexico, Nankai Trough off the eastern coast of Japan, Blake Ridge in the northwestern Atlantic Ocean, the Cascadia Margin in the northeastern Pacific Ocean, and the Haakon-Mosby Mud Volcano (MV) in the Norwegian-Greenland Sea (Fig. 7).

Research Approach: Key program efforts at NRL includes integration of: geoacoustical surveys to predict hydrate locations; methane sensors to trace hydrate rich regions in the ocean floor; field and laboratory analysis of hydrate structure and content; and stable and radio carbon isotope analysis to assist in the interpretation of methane sources and understanding of the hydrate content and stability. The following sections describe Code 6000's efforts in this project.

Testing and Development of a Methane Sensor: Methane sensing is applied to identify po-

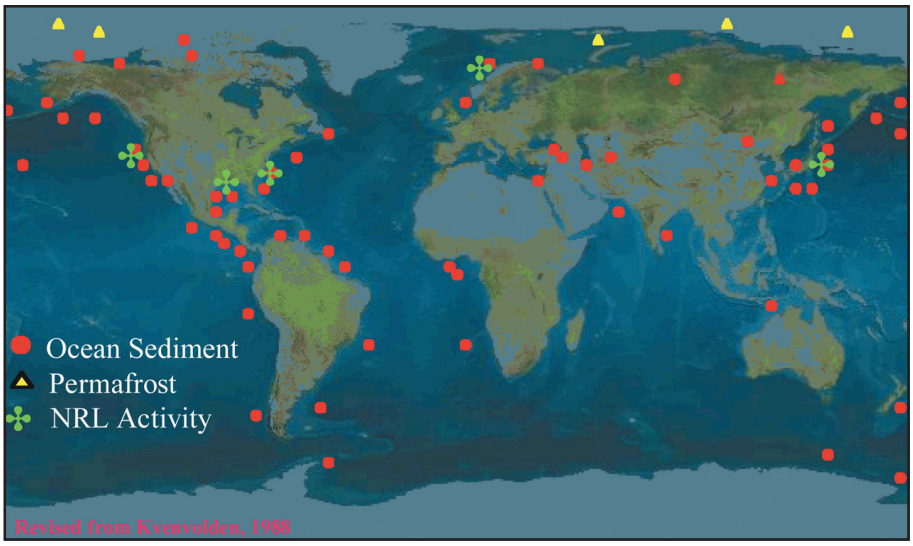

FIGURE 7
World methane hydrate distribution in the ocean, Arctic region. NRL regions of interest are highlighted around the U.S., Canada, Norway, and Japan.

tential hydrate-rich regions in the sediments and to study the flow of methane from these regions into the water column. A methane sensor, METS, from ASD Sensortechnik Gmgh (Germany) became commercially available at the start of the Methane Hydrate Advanced Research Initiative (ARI). The METS sensor specifications list an operational depth range from 0 to 2000 m, temperature range of 0 to 40 °C, and a methane concentration range of 50 nmol/l to 10 µmol/l. The methane sensor is a semiconductor (metal oxide) that works on the principle of hydrocarbon adsorption. The data collected during the summer 2000 cruise to the Gulf of Mexico was obtained from one sensor, D21. The METS sensor was placed on the forward platform of the submersible in view of the operator. This allowed the operator and observer to properly annotate the sampling events since multiple experiments were ongoing on each dive. Figure 8 shows data collected while working with hydrate mounds or with pieces of hydrate. Methane concentrations rise from a background level of ~0.1 µmols/l to a high of ~8.8 µmols/l. The first peak (~2.1 µmols/l) at 5,788 seconds was obtained when working around a loose piece of hydrate. While working a hydrate mound at 6,634 seconds, a concentration of ~2.9 µmols/l was obtained. The highest con-

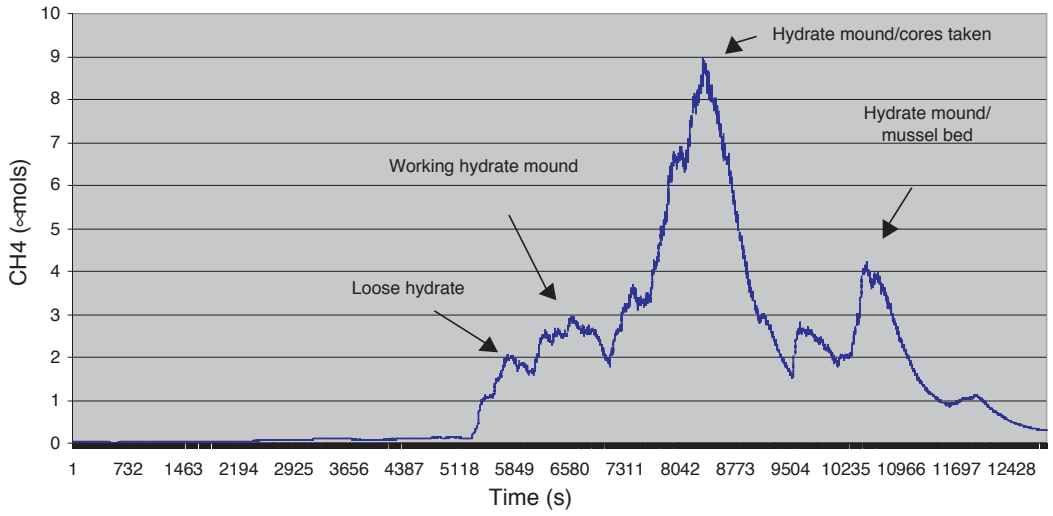

FIGURE 8
This plot shows that high methane concentrations can be observed with the methane sensor in the vicinity of hydrate outcroppings. Work was conducted on submarine dives in the Gulf of Mexico.

centration (~9 µmols/l) occurred while cores were being taken in a hydrate mound. The peak located at 10,523 seconds occurred while working in a mussel bed located to the left of the hydrate mound.

Analysis of Hydrate Methane Sources, Structure, and Content: The formation, stability and required dissociation energy in hydrates varies as a function of physical, biological, and chemical factors. The chemical and biological parameters are a major effort in methane hydrate research conducted by Code 6000 scientists. For analysis of the hydrate gas sources, scientists at NRL are applying carbon isotope analysis to differentiate between thermogenic and biogenic gas sources. We find a broad range of gases in the hydrates (Table 1), and the methane source in the hydrates varies at different sites between biogenic and thermogenic origin (Fig. 9). In Fig. 9 gases with more negative values (below –50 ‰) are more influenced by biogenic cycles; above this value, more thermogenic methane is present. The carbon isotope data for the higher molecular weight gases do not show large variation. These have isotope signatures indicating a thermogenic origin.

We couple the carbon isotope analysis with a survey of the hydrate structure. Currently two approaches for structural analysis are being applied: proton nuclear magnetic resonance (NMR) and x-ray diffraction (in conjunction with Argonne National Laboratory). High-pressure and low-temperature x-ray diffraction at the Advanced Photon Source at Argonne National Laboratory has examined the possible presence of structure H hydrate in natural hydrate material. Figure 10 shows peaks that may originate from structure H (red labels), but additional peaks appear to arise from structure I or II hydrate, or water ice Ih (blue, cyan, and green labels, respectively). Further analysis is needed to verify the presence of structure H hydrate. Such a result would confirm the incorporation of higher mass hydrocarbons into the hydrate structure (Table 1). More detailed structure analysis and thermal expansion and bulk modulus measurements are underway that will document this information for the first time for natural hydrate material.

This research contributes to understanding methane hydrate formation, content, and stability. NRL collaborations with scientists at industry, government,

Table 1 — Methane Hydrate Content in Samples from the Texas-Louisiana Shelf in the Gulf of Mexico and the Haakon-Mosby Mud Volcano in the Norwegian Greenland Sea. Bush Hill and Green Canyon are Located in the Gulf of Mexico. Yellow Hydrates Have Petroleum Present Between the Clathrate Structures.

Sample ID	% Hydrocarbon Composition						
	C_1	C_2	C_3	$i-C_4$	C_4	C_5	C_6
Haakon Mosby MV	99.5	0.1	0.1	0.1	0.1	0.0	0.1
Bush Hill White	72.1	11.5	13.1	2.4	1.0	0.0	0.0
Bush Hill Yellow	73.5	11.5	11.6	2.0	1.0	0.1	0.2
Green Canyon White	66.5	8.9	15.8	7.2	1.4	0.1	0.1
Green Canyon Yellow	69.5	8.6	15.2	5.4	1.2	0.0	0.0
Bush Hill	29.7	15.3	36.6	9.7	4.0	3.2	1.6

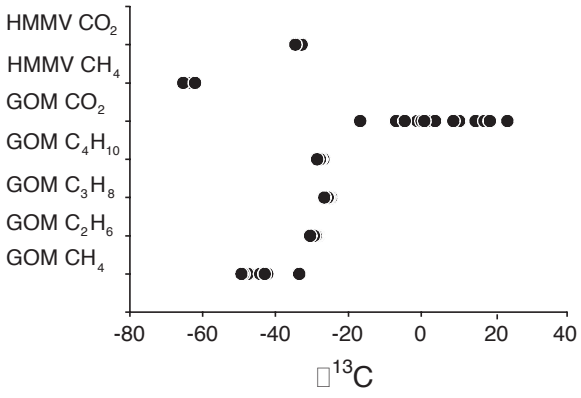

FIGURE 9
Stable carbon isotope data for carbon gases in hydrates taken on submarine dives on the Texas-Louisiana Shelf in the Gulf of Mexico (GOM) and the Haakon-Mosby Mud Volcano (HMMV) in the Norwegian Greenland Sea. Carbon isotope data include compounds ranging from methane to butane and carbon dioxide.

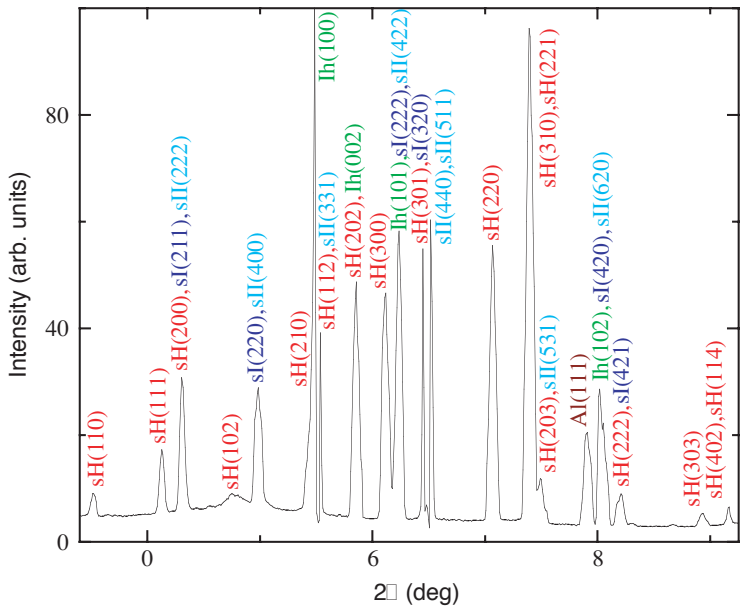

FIGURE 10
X-ray diffraction of natural hydrate collected from the Gulf of Mexico. Measurement performed at 500 psi and 150 K using 33 keV (0.3757 Å) photons from the Advanced Photon Source. Diffraction peaks labeled from hydrate structure H (red), structure I (blue), and structure II (cyan), and water ice Ih (green).

and university facilities throughout the United States, Canada, Norway, Japan, Korea, and Russia address topics in future energy, ocean floor fuel cell development, coastal stability, ocean carbon cycling, and global warming.

Acknowledgments: The NRL research program is an Advance Research Initiative, "Alteration of Sediment Properties Through Dissociation of Gas Hydrates." Use of the Advanced Photon Source was supported by the U.S. Department of Energy, Basic Energy Sciences, Office of Science.

[Sponsored by NRL]

Study of Microbial Chromium(VI) Reduction by Electron Energy Loss Spectroscopy

T.L. Daulton,[1] B.J. Little,[2] and J.M. Jones-Meehan[3]
[1]*Marine Geosciences Division*
[2]*Oceanography Division*
[3]*Chemistry Division*

Introduction: The geochemistry and toxicity of chromium (Cr) are controlled by valence state. Chromium is a redox active 3*d* transition metal with a wide range (–2 to +6) of possible oxidation states, of which only two are stable. Thermodynamic calculations predict that soluble Cr(VI) is energetically favored for oxic conditions, while insoluble Cr(III) is favored under anoxic or suboxic conditions. Hexavalent chromium species are strong oxidants that act as carcinogens, mutagens, and teratogens in biological systems. Therefore, microbial Cr(VI) reduction is of particular technological and biological importance because it converts a toxic, mobile element into a less toxic, immobile form.

Study of microbial Cr(VI) reduction, such as identification of reduction intermediates, has been hindered by the lack of analytical techniques that can identify oxidation state with subcellular spatial resolution. The most common method for measuring Cr(VI) reduction in bacterial cultures is the diphenylcarbazide colorimetric assay in which Cr(VI) concentration is determined from absorbance at 540 nm by the stoichiometric oxidation products of diphenylcarbazide reagent. However, this bulk technique cannot provide the submicron-scale information necessary for understanding microbial reduction processes. One technique with sufficient spatial resolution is electron energy loss spectroscopy (EELS). EELS directly measures the energy loss of incident electrons that inelastically scatter from atoms in the specimen and is a direct probe of the electron configuration around atoms. Consequently, EELS can identify the oxidation state of 3*d* and 4*d* transition metals.[1] Despite the detailed, submicron-scale infor-

mation EELS techniques can provide on oxidation state, they have never been applied in microbial reduction studies. This article demonstrates the application of EELS for the determination of metal oxidation state in studies of microbial reduction. Specifically, we examined reduction of Cr(VI) in anaerobic cultures of *Shewanella oneidensis* containing $Cr(VI)O_4^{2-}$. *S. oneidensis* is a gram-negative, facultative bacterium, capable of respiring aerobically and anaerobically by using a variety of terminal electron acceptors.[2] It is a member of the γ-subclass of *Proteobacteria,* and has been isolated from lascustrine and marine environments.

Methodology: Determination of oxidation state by EELS is accomplished by analyzing valence-induced differences in fine structure of L_2 and L_3 (or collectively $L_{2,3}$) absorption edges. The $L_{2,3}$ absorption edges arise from transitions to unoccupied *d* levels from two spin-orbit split levels: the $2p_{1/2}$ level (producing the L_2 edge) and the $2p_{3/2}$ level (producing the L_3 edge). The valence of a transition metal is related to the number of holes in the *d* level, i.e., the $3d^n$ (or $4d^n$) configuration. For example, tetrahedral Cr(VI) has an empty *d* orbital ($3d^0$ configuration) and octahedral Cr(III) has a $3d^3$ configuration. Since $L_{2,3}$ absorption edges are inherently dependent on the number of unoccupied *d* levels in 3*d* and 4*d* transition metals, they are sensitive to valence state.

Bacterial cultures were examined directly by environmental cell (EC)-transmission electron microscopy (TEM) at 100 Torr, under a circulation of air saturated with water vapor. The EC-TEM system is of the closed-cell type. A pressurized environment is maintained by two electron-transparent, amorphous-carbon windows with the specimen supported on the lower window. Bacteria were also examined in cross section by conventional TEM after embedding and thin sectioning.

Results: Examination by EC-TEM shows the typical rod-shaped morphology of *S. oneidensis.* In particular, the bacterial membranes are intact and do not show evidence of rupture by partial decompression. Cells remain plump/hydrated, while extracellular polymeric substances encapsulating the cells retain moisture. Electron microscopy reveals two distinct populations of *S. oneidensis* in incubated cultures containing Cr(VI): cells that exhibit low image contrast (Fig. 11(a)) and heavily precipitate-encrusted cells that exhibit high image contrast (Figs. 11(b)).

Several EELS techniques were applied to determine the oxidation state of Cr associated with the encrusted cells. Oxidation state was determined by measuring the chemical shift and intensity ratios of Cr-$L_{2,3}$ adsorption peaks.[3] Figure 12 compares the EELS spectra of encrusted, hydrated *S. oneidensis* collected by EC-TEM to that of Cr oxidation-state standards collected by conventional TEM. The correlation between measured L_3/L_2 integrated-peak intensity ratios and L_3 peak positions for standards demonstrates that different oxidation states fall within well-separated regions (Fig. 13). Within a given oxidation state, spectra of individual standards fall within separate groupings, reflecting possible differences in atom coordination, spin-orbit interactions, and crystal field splitting. Comparison with the standards demonstrates that precipitate-encrusted bacteria contain Cr in oxidation state +3 or lower (Fig. 13). Precipitates encrusting bacteria were also examined in cross section. EELS measurements by conventional TEM of cross sections (Fig. 13) are consistent with measurements of encrusted, hydrated bacteria by EC-TEM, demonstrating that EELS provides accurate data, even under the more onerous experimental conditions of the EC.

Summary: Chemical and oxidation state information for the microbial reduction of Cr(VI) by the

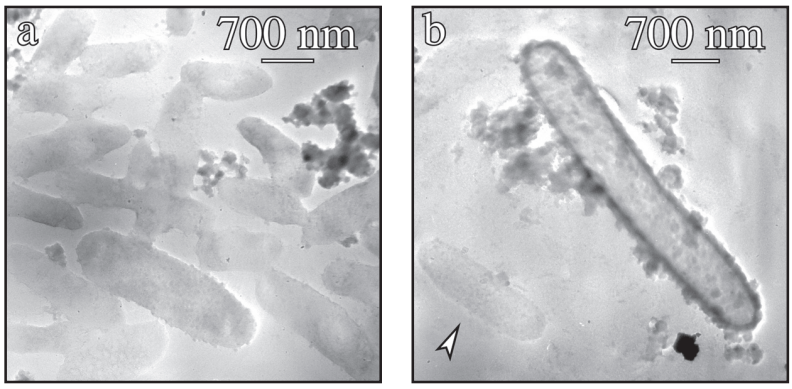

FIGURE 11
Shewanella oneidensis imaged by EC-TEM at 100 Torr: bacteria (a) exhibiting low contrast and (b) encrusted with electron dense precipitates. Arrowhead in (b) points to a low contrast bacterium, illustrating the dramatic contrast difference with respect to encrusted bacteria.

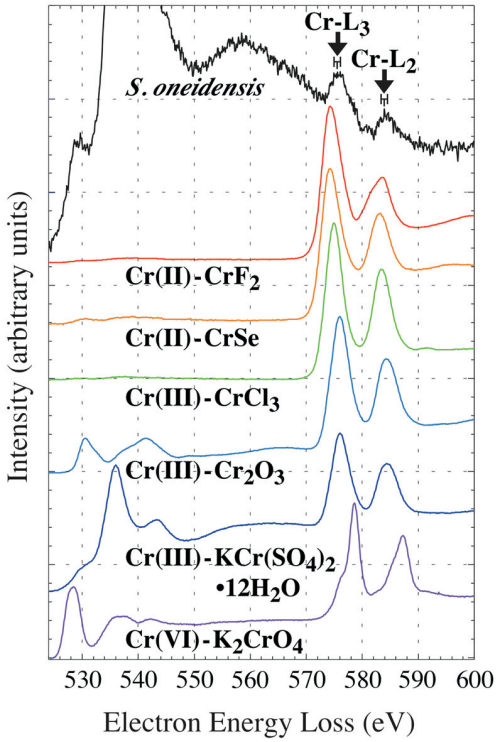

FIGURE 12
Comparison of EELS spectra of encrusted *Shewanella oneidensis* in the EC and Cr oxidation-state standards. Spectra were normalized to the intensity of the L_3 peak and offset from one another.

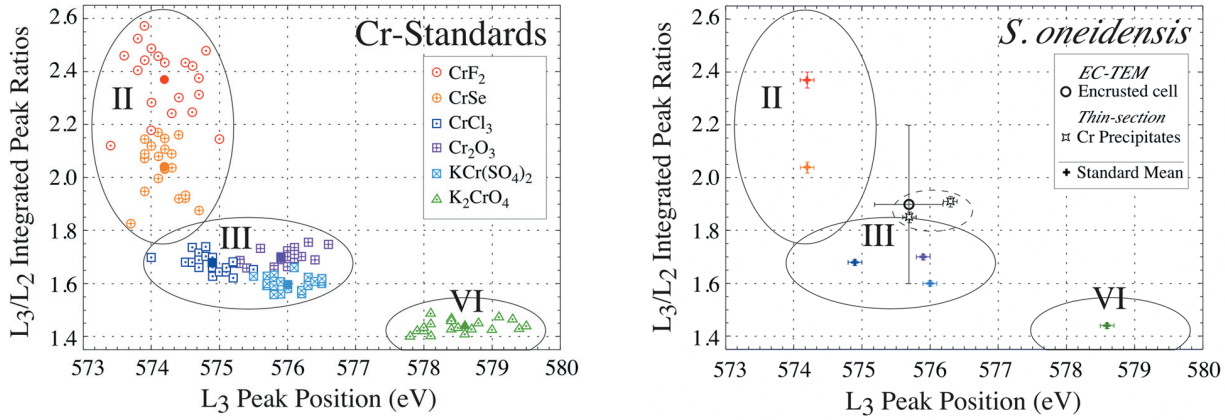

(a) (b)

FIGURE 13
Correlation between measured L_3/L_2 integrated-peak ratios and L_3 peak positions (a) Cr oxidation-state standards, (b) bacteria and precipitates (solid data points represent the mean of the data for a particular Cr standard).

facultative anaerobe *Shewanella oneidensis* was acquired with high spatial resolution using EELS. We demonstrate that quantitative measurements of oxidation state can be performed on hydrated specimens by EC-TEM. This is the first time the oxidation state of microbial metal-reduction products, localized with bacteria, has been measured. Such information is vital for identifying microbial electron transfer sites and transfer mechanisms.

[Sponsored by ONR]

References

[1] R.F. Egerton, *Electron Energy-loss Spectroscopy in the Electron Microscope* (Plenum, New York, 1996).

[2] K. Venkateswaran, D.P. Moser, M.E. Dollhopf, D.P. Lies, D.A. Saffarini, B.J. MacGregor, D.B. Ringelberg, D.C. White, M. Nishijima, H. Sano, J. Burghardt, E. Stackebrandt, and K.H. Nealson, "Polyphasic Taxonomy of the Genus *Shewanella* and Description of *Shewanella oneidensis* sp. nov.," *Int. J. Syst. Bacteriol.* **49**, 705-724 (1999).

[3] T.L. Daulton, B.J. Little, K. Lowe, and J. Jones-Meehan, "In-situ Environmental Cell -Transmission Electron Microscopy Study of Microbial Reduction of Chromium(VI) using Electron Energy Loss Spectroscopy," *Microscopy Microanal.*, in press.